Ionization Rates in a Bose-Einstein Condensate of Metastable Helium

O. Sirjean, S. Seidelin, J. Viana Gomes,* D. Boiron, C. I. Westbrook, and A. Aspect
Laboratoire Charles Fabry de l'Institut d'Optique, UMR 8501 du CNRS, F-91403 Orsay Cedex, France

G. V. Shlyapnikov
FOM Institute for Atomic and Molecular Physics, Kruislaan 407, 1098 SJ Amsterdam, The Netherlands and Russian Research Center Kurchatov Institute, Kurchatov Square, 123182 Moscow, Russia
(Received 5 August 2002; published 12 November 2002)

We have studied ionizing collisions in a BEC of metastable He. Measurements of the ion production rate combined with measurements of the density and number of atoms for the same sample allow us to estimate both the two- and three-body contributions to this rate. A comparison with the decay of the atom number indicates that ionizing collisions are largely or wholly responsible for the loss. Quantum depletion makes a substantial correction to the three-body rate constant.

DOI: 10.1103/PhysRevLett.89.220406 PACS numbers: 34.50.–s, 05.30.–d, 67.65.+z, 82.20.Pm

The observation of Bose-Einstein condensation (BEC) of metastable helium (He in the 2^3S_1 state, denoted He*) [1,2] constituted a pleasant surprise for experimentalists although the possibility had been predicted theoretically [3]. Success hinged, among other things, on a strong suppression of Penning ionization in the spin-polarized, magnetically trapped gas. Too high a rate of ionization would have prevented the accumulation of sufficient density to achieve evaporative cooling. The ionization rate is not completely suppressed however, and when the atomic density gets high enough, a magnetically trapped sample of He* does produce a detectable flux of ions. As shown in [1], this signal can even be used as a signature of BEC. The observation of ions from the condensate opens the possibility of monitoring in real time the growth kinetics of a condensate [4]. This is an exciting prospect, but to quantitatively interpret the ion rate, one needs the contributions of two- and three-body collisions.

In this paper we use the unique features of metastable atoms to detect, in a single realization, the ionization rate, the density, and the atom number. This allows us to extract two- and three-body rate constants without relying on fits to nonexponential decay of the atom number, which require good experimental reproducibility [5–7] and are difficult to interpret quantitatively [5]. After estimating the ionization rate constants, a comparison with the decay of the atom number reveals no evidence for collisional avalanche processes. Thus, by contrast with ^{87}Rb [8], He* seems to be a good candidate for studying the "hydrodynamic" regime [9], as well as the effects of quantum depletion, i.e., a departure from the Gross-Pitaevskii wave function in the Bogoliubov theory, due to atomic interactions [10]. Indeed in our analysis of the three-body ionization process, quantum depletion makes a substantial correction [11].

Much theoretical [3,12] and experimental [1,2,13,14] work has already been devoted to estimating inelastic decay rates in He*. The dominant two-body decay mechanisms, called Penning ionization,

$$\mathrm{He}^* + \mathrm{He}^* \rightarrow \begin{cases} \mathrm{He}^+ + \mathrm{He}(1S) + e^- \\ \mathrm{He}_2^+ + e^- \end{cases} \quad (1)$$

are known to be suppressed by at least 3 orders of magnitude in a spin-polarized sample, but the total rate constant has not yet been measured. The three-body reaction,

$$\begin{aligned} \mathrm{He}^* + \mathrm{He}^* + \mathrm{He}^* &\rightarrow \mathrm{He}_2^* + \mathrm{He}^*(\sim 1\ \mathrm{mK}) \\ &\hookrightarrow \mathrm{He}^+ + \mathrm{He}(1S) + e^- \end{aligned} \quad (2)$$

proceeds via three-body recombination followed by autoionization of the excited molecule. Both reactions yield one positive ion which is easily detected. We define collision rate constants according to the density loss in a thermal cloud: $\frac{dn}{dt} = -\frac{n}{\tau} - \beta n^2 - Ln^3$ with n the local density, τ the (background gas limited) lifetime of the sample, and β and L the two-body and three-body ionization rate constants defined for a thermal cloud [15]. The theoretical estimates of the rate constants at 1 μK are $\beta \sim 2 \times 10^{-14}\ \mathrm{cm^3\,s^{-1}}$ [3,12] and $L \sim 10^{-26}\ \mathrm{cm^6\,s^{-1}}$ [16], and the experimental upper limits were [1,2] $\beta \leq 8.4 \times 10^{-14}\ \mathrm{cm^3\,s^{-1}}$ and $L \leq 1.7 \times 10^{-26}\ \mathrm{cm^6\,s^{-1}}$.

For a pure BEC, in the Thomas-Fermi regime with a number of atoms N_0, and a peak density n_0, one can calculate the expected ionization rate per trapped atom:

$$\Gamma = \frac{\text{ion rate}}{N_0} = \frac{1}{\tau'} + \frac{2}{7}\kappa_2 \beta n_0 + \frac{8}{63}\kappa_3 L n_0^2. \quad (3)$$

The numerical factors come from the integration over the parabolic spatial profile and the fact that although two or three atoms are lost in each type of collision, only one ion is produced. The effective lifetime $\tau' \geq \tau$ is due to *ionizing* collisions with the background gas. The factors κ_i take into account the fact that the two- and three-particle local correlation functions are smaller than those of a

thermal cloud. For a dilute BEC $\kappa_2 = 1/2!$ and $\kappa_3 = 1/3!$ [7,11]. Because the He* scattering length (a) is so large, quantum depletion ($\sim \sqrt{n_0 a^3}$) leads to significant corrections [11] to the κ's as we discuss below.

Much of our setup has been described previously [1,17,18]. Briefly, we trap up to 2×10^8 atoms at 1 mK in a Ioffe-Pritchard trap with a lifetime (τ) of 90 s. We use a "cloverleaf" configuration [19] with a bias field $B_0 =$ 150 mG. The axial and radial oscillation frequencies in the harmonic trapping potential are $\nu_\parallel = 47 \pm 3$ Hz and $\nu_\perp = 1800 \pm 50$ Hz, respectively [$\overline{\omega}/2\pi = (\nu_\parallel \nu_\perp^2)^{1/3} =$ 534 Hz]. A crucial feature of our setup is the detection scheme, based on a two stage, single anode microchannel plate detector (MCP) placed below the trapping region. Two grids above the MCP allow us either to repel positive ions and detect only the He* atoms, or to attract and detect positive ions produced in the trapped cloud.

To detect the ion flux, the MCP is used in counting mode: the anode pulses from each ion are amplified, discriminated with a 600 ns dead time and processed by a counter which records the time delay between successive events. Typical count rates around BEC transition are between 10^2 and 10^5 s^{-1}. We have checked that the correlation function of the count rate is flat, indicating that there is no double counting nor any significant time correlation in the ion production. The dark count rate is of order 1 s^{-1}. By changing the sign of the grid voltage, we have checked that while counting ions, the neutral He* detection rate is negligible compared to the ion rate (less than 5%) even when the radio frequency (rf) shield is on. The intrinsic ion detection efficiency of the MCP for 2 keV He^+ ions is close to the open area ratio (60%) [20]. To estimate the total ion detection efficiency, we then multiply by the geometric transmission of the two grids $(0.84)^2$. Based on Refs. [20,21], we assume this (0.42) is an upper limit on our detection efficiency.

To find the values of N_0 and n_0 corresponding to the measured ion rate, we use the MCP to observe the time-of-flight (TOF) signal of the He* atoms released from the rapidly switched off trap. The instantaneous count rate can be as high as 10^6 s^{-1}, and the MCP saturates when used in counting mode. To avoid this problem, we lower the MCP gain, and record the TOF signal in analog mode with a time constant of 400 μs. Several tests were performed to verify the linearity of the detector.

In a typical run, evaporative cooling takes place for 40 s, down to an rf-knife frequency about 50 kHz above the minimum of the trapping potential. Near the end of the ramp, the ion rate increases sharply, signaling the appearance of a BEC (Fig. 4 in [1]). After reaching the final value, the rf knife is held on at that frequency. This constitutes an rf shield which eliminates hot atoms and maintains a quasipure BEC for up to 15 s (see Fig. 3). By quasipure we mean that we see no thermal wings in signals such as shown in the inset of Fig. 1. From tests of our fitting procedure, we estimate that the smallest thermal fraction we can distinguish is about 20%, with a temperature on the order of the chemical potential. Runs with visible thermal wings were discarded.

To acquire the TOF signals corresponding to a given ion rate, we turn off the rf shield, wait 50 ms, and then turn off the magnetic trap and switch the MCP to analog mode. To be sure that the rf has no influence on the ion rate, we use only the number of ions observed during the 50 ms delay to get the rate. We fit the TOF signals to an inverted parabola squared as expected for a pure BEC in the Thomas-Fermi regime and for a TOF width ($\sim$ 5 ms) narrow compared to the mean arrival time (100 ms) [1]. Under these assumptions, the chemical potential μ depends only on the TOF width, the atomic mass, and the acceleration of gravity [22], and thus can be measured quite accurately. Figure 1 shows that μ varies as expected as $N_d^{2/5}$ with N_d the number of detected atoms in the quasipure BEC. A fit on a log-log plot gives a slope of 0.39. Residuals from the linear fit do not show any systematic variation which is a good indication of the detection linearity and of the proportionality between N_d and N_0.

To determine the collision rate constants β and L, we need an absolute calibration of the number of atoms and the density. As discussed in Ref. [1], all the atoms are not detected, and the direct calibration has a 50% uncertainty which is responsible for the large uncertainty in the scattering length a. In fact the measurement of the chemical potential gives an accurate value for the product $n_0 a = \mu m/4\pi\hbar^2$, and with the value of $\overline{\omega}$ gives the product $N_0 a = (1/15)(\hbar/m\overline{\omega})^{1/2}(2\mu/\hbar\overline{\omega})^{5/2}$ as well. Therefore, in the hopes that the He* scattering length will be measured more accurately in the future, we shall express N_0 and n_0 in terms of a. In this paper, unless stated otherwise, we suppose that $a = 20$ nm, and in our conclusions we shall discuss how our results depend on a.

Figure 2 shows the ion rate per atom Γ versus the peak density. The densest sample corresponds to $N_0 = 2 \times 10^5$

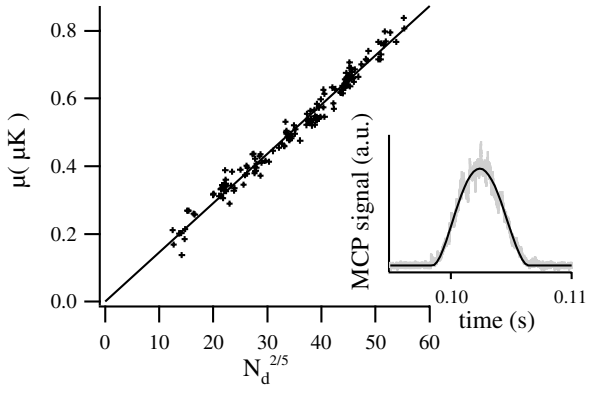

FIG. 1. Chemical potential versus number of detected atoms to the power $\frac{2}{5}$ and its linear fit. Data are for quasipure BEC. The inset shows a typical TOF signal and its inverted parabola squared fit.

atoms and $n_0 = 2.5 \times 10^{13}$ cm^{-3}. The corresponding Thomas-Fermi radii are $r_\perp \simeq 5$ μm and $r_\parallel \simeq 200$ μm. The vertical intercept in Fig. 2 corresponds to ionizing collisions with the background gas ($1/\tau'$). We have independently estimated this rate using trapped thermal clouds at 1 mK and 5 μK and found $1/\tau' \lesssim 5 \times 10^{-3}$ s^{-1}. This value is negligible at the scale of the figure.

The curvature in Fig. 2 shows that three-body ionizing collisions are significant. Before fitting the data to get β and L, we must take into account several effects. First, for three-body collisions, quantum depletion is important. For $T = 0$, on the basis of Ref. [11], we obtain a multiplicative correction to the factor κ_3 of $(1 + \epsilon) = (1 + 23.2 \times \sqrt{n_0 a^3})$ [23]. At our highest density $\epsilon \simeq 0.35$. Two-body collisions are subject to an analogous correction but approximately 3 times smaller. The fits in Fig. 2 include the density dependence of $\kappa_{2,3}$, associated with quantum depletion. The $n_0^{3/2}$ dependence introduced for two-body collisions is far too small to explain the curvature in the data. The density dependence of $\kappa_{2,3}$ does not improve the quality of the fit, but it significantly reduces the value of the fitted value of L (by 30%).

In addition, the fact that the sample probably contains a small thermal component means that collisions between the condensed and the thermal parts must be taken into account [6,11]. Assuming a 10% thermal population ($\frac{\mu}{k_B T} \simeq 1.5$), we find $\kappa_3 = \frac{1}{6}(1 + \epsilon + \epsilon')$, with an additional correction $\epsilon' \simeq 0.11$ for the densest sample [24].

Taking into account all these corrections, and assuming an ion detection efficiency of 0.42, the fitted values of the collision rate constants [15] are $\beta_{20} = 2.9(\pm 2.0) \times 10^{-14}$ cm^3 sec^{-1} and $L_{20} = 1.2(\pm 0.7) \times 10^{-26}$ cm^6 sec^{-1}, where the subscripts refer to the assumed value of a. These values are in good agreement with the theoretical estimates. The error bars are estimated as follows. We fix either β or L and use the other as a fit parameter. We repeat this procedure for different values of the fixed parameter and take the range over which we can get a converging and physically reasonable fit (i.e., no negative rate constants) as the uncertainty in the fixed parameter. These error bars are highly correlated since if β is increased, L must be decreased and vice versa. The error bars do not include the uncertainty in the absolute ion detection efficiency (see below).

Until now we have assumed $a = 20$ nm, but current experiments give a range from 8 to 30 nm [1,2]. Using Eq. (3) and our parametrization of n_0 and N_0 in terms of a, one can see that, in the absence of quantum depletion, the values of β and L extracted from our analysis would be proportional to a^2 and a^3, respectively. Taking quantum depletion into account, no simple analytical dependence exists, but one can numerically evaluate β and L vs a and fit the results to expansions with leading terms in a^2 and a^3, respectively. The effect of quantum depletion is negligible for β [$\beta_a \approx \beta_{20}(\frac{a}{20})^2$]. For L, we find $L_a \approx L_{20}(\frac{a}{20})^3[1 - 0.21\frac{a-20}{20}]$ with a in nm.

To test the consistency of our measurements, we plot the decay of the atom number (Fig. 3). To acquire these data, we held the BEC in the trap in the presence of the rf shield for varying times. This study involves multiple BEC realizations, which typically exhibit large fluctuations in the initial atom number. We have been able to reduce this noise by using the ion signal to select only data corresponding to the same ion rate 500 ms after the end of the ramp. This time corresponds to $t = 0$ in the figure. We also plot the predicted decay curve (solid line) corresponding to ionization only. This curve results from a numerical integration of the atom loss due to ionization processes, calculated from the fitted values β_{20} and L_{20}. The fact that the error bars on β and L are correlated

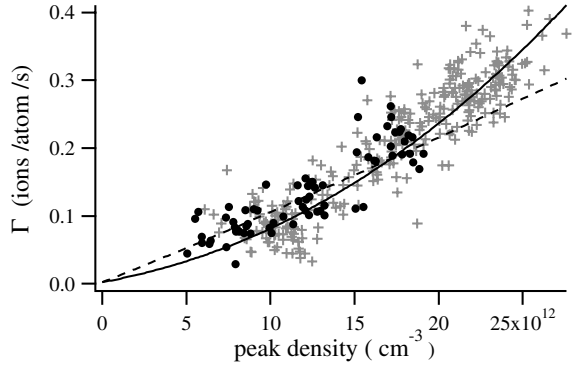

FIG. 2. Ion rate per trapped atom versus peak density for 350 different quasipure BEC's. Atom number and density are deduced from μ, $\overline{\omega}$, and a (here 20 nm). Data were taken for two different bias fields corresponding to $\nu_\perp = 1800$ Hz (crosses) and $\nu_\perp = 1200$ Hz (circles). The dashed line corresponds to the best fit involving only two-body collisions. The solid line is a fit to two- and three-body processes.

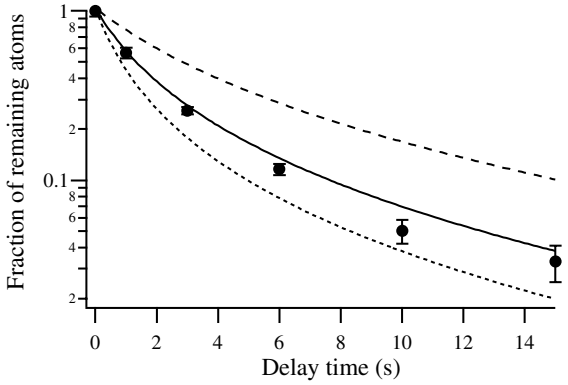

FIG. 3. Fraction of remaining atoms measured by TOF as a function of time. The rf shield is on and the cloud remains a quasipure condensate during the decay. The lines correspond to the predicted atom decay according to Eq. (3) with the fitted value of the two- and three-body rate constants for $a = 10$ nm (dashed line), $a = 20$ nm (solid line), and $a = 30$ nm (dotted line). The case of $a = 10$ nm is not necessarily excluded because other, nonionizing losses could be present.

leads to a small uncertainty on the solid curve that happens to be of the same order of magnitude as the typical error bars on the data. The observed decay agrees fairly well with the solid curve, and ionization apparently accounts for most of the loss. If the ion detection efficiency were actually lower than we assume, the predicted decay would be faster than the observed decay which is unphysical (assuming $a = 20$ nm). We conclude that our estimate of the ion detection efficiency is reasonable and does not lead to an additional uncertainty in β and L.

We also plot the curves obtained from the same analysis but with scattering lengths of 10 and 30 nm, assuming a detection efficiency of 0.42. The curve corresponding to $a = 30$ nm lies below the data points. Based on our analysis, this means that $a = 30$ nm is excluded. A scattering length of 25 nm is the largest one consistent with our data. In contrast, the decay predicted for an analysis with $a = 10$ nm is slower than the observed decay. This would mean that there are additional nonionizing losses (contributing up to half of the total loss), and/or that we have overestimated the ion detection efficiency by a factor as large as 2. In the latter case, β and L should be multiplied by the same factor. This results for $a = 10$ nm in a supplementary systematic uncertainty on β and L of a factor as large as 2.

In the event that our upper limit on the ion detection efficiency is too low, the rate constants β and L should be reduced by a factor as large as 2.4 ($= 0.42^{-1}$). In that case, our data would not exclude $a = 30$ nm and nonionizing losses could significantly contribute to the total loss.

Even though the peak densities of our BEC are small compared to those in alkalis, the elastic collision rate is high because of the large scattering length, and one must consider the possibility of collisional avalanches. For $a = 20$ nm our densest cloud has a mean free path of 7 μm and using the definition of [8] the collisional opacity is 0.8. With Rb atoms this would result in much increased loss due to avalanches [8]. Here we have to consider secondary collisions leading to both ion production and atom loss. However, for secondary ionization, mean free paths are at least 2 orders of magnitude larger than $r_{\parallel}$. Hence secondary ionization is unimportant. This conclusion is supported by our observation of no correlation in the time distribution of detected ions.

The good agreement between the data and the curve in Fig. 3 indicates that losses due to nonionizing collisional avalanches are not taking place either. This is in agreement with data on elastic collisions with He^+, He_2^+, and He($1S$), which have small cross sections [25]. Collisions with hot He* atoms from the reaction of Eq. (2) are more likely to play a role, but due to the higher velocity, the elastic cross section for these atoms is smaller. In Rb the situation is different because a d-wave resonance increases the total cross section [8].

The theoretical analysis shows that quantum depletion strongly affects the measured three-body rate constant. One way to experimentally demonstrate this effect would be to compare with similar measurements with thermal clouds. Absolute calibration of ion and atom detection efficiency should play no role in this comparison, if one could prove that they are the same for both situations.

We thank F. Gerbier for stimulating discussions. This work was supported by the European Union under Grants No. IST-1999-11055 and No. HPRN-CT-2000-00125, and by the DGA Grant No. 00.34.025.

*Permanent address: Departamento de Fisica, Universidade do Minho, Campus de Gualtar, 4710-057 Braga, Portugal.

[1] A. Robert *et al.*, Science **292**, 461 (2001).
[2] F. Pereira Dos Santos *et al.*, Phys. Rev. Lett. **86**, 3459 (2001); F. Pereira Dos Santos *et al.*, Eur. Phys. J. D **19**, 103 (2002).
[3] G.V. Shlyapnikov *et al.*, Phys. Rev. Lett. **73**, 3247 (1994); P.O. Fedichev *et al.*, Phys. Rev. A **53**, 1447 (1996).
[4] H.J. Miesner *et al.*, Science **270**, 1005 (1998); M. Köhl *et al.*, Phys. Rev. Lett. **88**, 080402 (2002).
[5] J.L. Roberts *et al.*, Phys. Rev. Lett. **85**, 728 (2000).
[6] J. Söding *et al.*, Appl. Phys. B **69**, 257 (1999).
[7] E.A. Burt *et al.*, Phys. Rev. Lett. **79**, 337 (1997).
[8] J. Schuster *et al.*, Phys. Rev. Lett. **87**, 170404 (2001).
[9] M. Leduc *et al.*, Acta Phys. Pol. B **33**, 2213 (2002).
[10] F. Dalfovo *et al.*, Rev. Mod. Phys. **71**, 463 (1999).
[11] Y. Kagan, B.V. Svistunov, and G.V. Shlyapnikov, JETP Lett. **42**, 209 (1985).
[12] V. Venturi *et al.*, Phys. Rev. A **60**, 4635 (1999); V. Venturi and I.B. Whittingham, Phys. Rev. A **61**, 060703(R) (2000).
[13] J.C. Hill *et al.*, Phys. Rev. A **5**, 189 (1972).
[14] N. Herschbach *et al.*, Phys. Rev. A **61**, 50 702 (2000).
[15] Collision rate constants are sometimes defined directly for a BEC ($\beta' = \beta/2$ and $L' = L/6$).
[16] P.O. Fedichev, M.W. Reynolds, and G.V. Shlyapnikov, Phys. Rev. Lett. **77**, 2921 (1996); P.F. Bedaque, E. Braaten, and H.W. Hammer, Phys. Rev. Lett. **85**, 908 (2000).
[17] A. Browaeys *et al.*, Phys. Rev. A **64**, 034703 (2001).
[18] S. Nowak *et al.*, Appl. Phys. B **70**, 455 (2000).
[19] M.O. Mewes *et al.*, Phys. Rev. Lett. **77**, 416 (1996).
[20] R.S. Gao *et al.*, Rev. Sci. Instrum. **55**, 1756 (1984).
[21] B. Deconihout *et al.*, Appl. Surf. Sci. **94/95**, 422 (1996).
[22] Y. Castin and R. Dum, Phys. Rev. Lett. **77**, 5315 (1996); Y. Kagan, E.L. Surkov, and G.V. Shlyapnikov, Phys. Rev. A **54**, R1753 (1996).
[23] The numerical factor $64/\sqrt{\pi}$ of [11] changes to 23.2 for a trapped bose gas.
[24] We have $\epsilon' = (\langle\langle 3n_0^2(n' + \alpha)\rangle\rangle + \langle 3n_0^2\langle n' + \alpha\rangle\rangle) \times \langle\langle n_0^3\rangle\rangle^{-1}$. The symbol $\langle\cdots\rangle$ denotes the integration over the condensate spatial region. The thermal part of the noncondensed density, n', and that of the anomalous average, α, are obtained in the local density approximation. This gives $\epsilon' = 7.7 \times \sqrt{n_0 a^3}$ for $(\mu/k_B T) = 1.5$.
[25] H.C.W. Beijerinck *et al.*, Phys. Rev. A **61**, 23 607 (2000).